10th International Symposium on the Science and Processing of Cast Iron – SPCI10

Non-metallic inclusions in lamellar graphite iron

V. Fourlakidis[1*], J. Ekengård[2] and A. Diószegi[3]
[1]Swerea SWECAST AB, P.O. Box 2033, SE-550 02 Jönköping, Sweden
[2]Sandvik SRP AB, Svedala, Sweden
[3]Jönköping University, Dept. of Mechanical Engineering/Material and Manufacturing Casting, Box 1026, SE-551 11 Jönköping, Sweden

Cast iron melts with two different carbon contents were used in this experiment. Quenched chill coins were extracted directly from the melting furnace and the size, the number and the composition of the non-metallic inclusions was examined using scanning electron microscopy (SEM), energy-dispersive X-ray spectroscopy (EDS) and an automate inclusions analysis system (EDAX). Large number of non-metallic inclusions was found in the chilled samples. Most of these inclusions are compounds of MnS with other elements. The number of the detected inclusions was found to increase with decreasing quenching temperature, while the number of large inclusions increases with the increase of the quenching temperature. This work provides supplementary data that helps a better understanding of the dependency between solidification rates, carbon composition, eutectic cells size, and constitutional undercooling in lamellar graphite iron.

Keywords: Lamellar graphite iron, MnS particles, graphite nucleation, non-metallic inclusions

Introduction

During the solidification of lamellar graphite iron the primary austenite is nucleated first and grows until the liquid metal attains the eutectic composition and the eutectic solidification occurs according to the stable austenite-graphite eutectic or the metastable austenite-iron carbide (cementite) eutectic. The equilibrium eutectic temperature for the austenite graphite reaction is tens of degrees higher than that of the austenite-carbide reaction in lamellar graphite iron. However the graphite nucleation usually requires significant undercooling below the eutectic temperature. When the undercooling becomes very high due to rapid cooling rates or low number of graphite nuclei, carbides formed instead of graphite [1-3].

In lamellar graphite iron the graphite phase nucleates heterogeneously from an un-dissolved graphite particle or from a complex substrate. The driving force for the graphite nucleation is the minimization of the free energy of the system consisting of the nuclei, the graphite and the melt. It has been shown that the value of the critical free energy is not available but is related to the lattice disregistry between nucleus and graphite. Therefore the disregistry can be used to indicate the ability of a surface to initiate the graphite nucleation [1].

Numerous research works investigate the phenomenon of graphite nucleation and the nature of the active nuclei at which the graphite nucleation can take place. Depending on the type of elements used for the treatment of the liquid iron, or the type of the inclusions which observed at the center of the graphite cells, several different graphite nucleation theories have been developed to explain the phenomena of heterogeneous nucleation of graphite in solidifying cast iron [5-12].

Lux [5] proposed that the addition of small amount of inoculation elements, such as Ca, Ba, Sr or Ce, in an iron melt promote the formation of salt-like carbides which constitute good nucleation sites for the participation of the graphite. Other researcher's [6] suggested that in flake graphite iron, CaO inclusions are nucleated first and they serve as embryo for the formation of SiO_2 oxide which possess as good nucleation site for the graphite.

Velichko [11] reconstructed a 3D visualization of the inclusions in a lamellar graphite iron sample. The performed EDS analysis indicated that those inclusions are precipitates of MnS. Wallace et al.[8] pointed out that the graphite flakes apparently grows from different sulfides inclusion. This theory is supported by Sommerfeld et al.[9] who analyzed the inclusions at the center of some eutectic cells and found that they consisting mainly by MnS. In another research work Riposan et al. [10] suggested that Al_2O_3 inclusions acting as nucleation sides for the precipitation of complex Mn(X)S compounds (where X is different elements such as Si, C, Ti, Ca, Al and others). These inclusions consider by the authors suitable sites for the nucleation of the graphite.

On the other hand the calculated lattice disregistry between the MnS inclusions and the graphite is very high (12.1%) and probably for this reason Tartera [5] consider that the MnS can serve as nucleation sites only in the absence of inoculation. Nevertheless the investigation results of other research works identified MnS as nucleus of flake graphite [9-10].

Sommerfeld et al. [9] used the software Thermo-Calc to calculate the fraction of stable phases in gray iron melts. The results of this work shows that in thermo-dynamical equilibrium condition the graphite is formed prior the MnS

* Corresponding author, e-mail: vasilios.fourlakidis@swerea.se

inclusions. MnS predicted to precipitate at temperature higher to graphite nucleation temperatures (1220°C), at high content of Mn and S (0.8% Mn and 0.12% S).

Recently [12], thermodynamics were used to analyze the nucleation of oxides and sulfides in lamellar graphite iron. This investigation shows that homogeneous nucleation of oxides/sulfides particles occurs when the concentration of oxygen/sulfur in the melt exceeding the supersaturation limit.

The aim of this experiment was to examine the number, the chemical composition and the size distribution of the non-metallic inclusions that forms in rapid solidify cast iron samples, produced at different quench temperatures.

Experimental Procedure

The experiment performed in an induction furnace having capacity of 6.000 Kg. The liquid iron was superheated up to 1500°C and then the melt left to cool down inside the furnace. Several chill samples were extracted from the melt during the cooling, until the liquid iron reaches the temperature of 1270°C.

The test samples are chilled coin shape specimens and they extracted directly from the melting furnace with the help of a resin bonded sand sampler. The rapid solidification of the samples it was provided by two steel plates which are positioned in the top and the bottom of the inner cavity of the sampler. The dimension of the experimental sample is ∅34.5x5.5 mm.

Two different carbon contents were used. The first melt had a carbon content of 2.8% and the second 3.2% C. Table 1 shows the chemical composition of the experimental alloys.

Table 1: Chemical compositions of the alloys, %wt.

Melt	C	Si	Mn	P	S	Cr	Cu	Al
1	3.4	1.7	0.5	0.04	0.05	0.2	0.7	0.003
2	3.7	1.7	0.6	0.05	0.05	0.2	0.7	0.003

The quenched specimens were ground and polished and number, size and chemical composition of the non-metallic inclusions measured by using SEM (Scanning Electron Microscope), EDS (Energy Dispersive Spectroscopy) system and an automate particles analysis program (EDAX Genesis software). Schamber [13] gives a detailed description of the methods used for the automated particle analysis in a SEM. An area of 0.026 mm² investigated in each specimen. The number of the analyzed micro-inclusions range from 130 to 870 particles per specimen.

Results and Discussion

The chemical composition of the alloy 1 in Table 1 has been used in JmatPro software for the calculation of the precipitated graphite and MnS, se Figure 1. The thermodynamic calculation shows that the graphite phase formed prior the precipitation of MnS in the specific alloy.

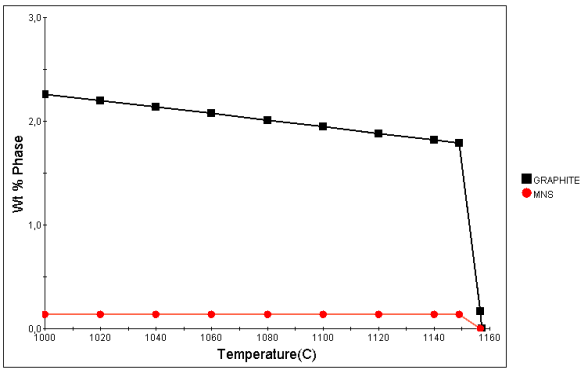

Fig. 1: Result of JmatPro calculation.

Large numbers of non-metallic inclusions were detected on the chilled samples. The majority of these inclusions are complex compounds of manganese and sulfur together with other elements such as O, Si, Ti, Ca, Al and others (Mn(X)S). Inclusions that contain manganese and sulfur alone (MnS) as well as oxides of various elements such as Ti, Si, Mn, Al and Ca were also detected. Figure 2 shows the number of the inclusions at various quenching temperatures and carbon compositions.

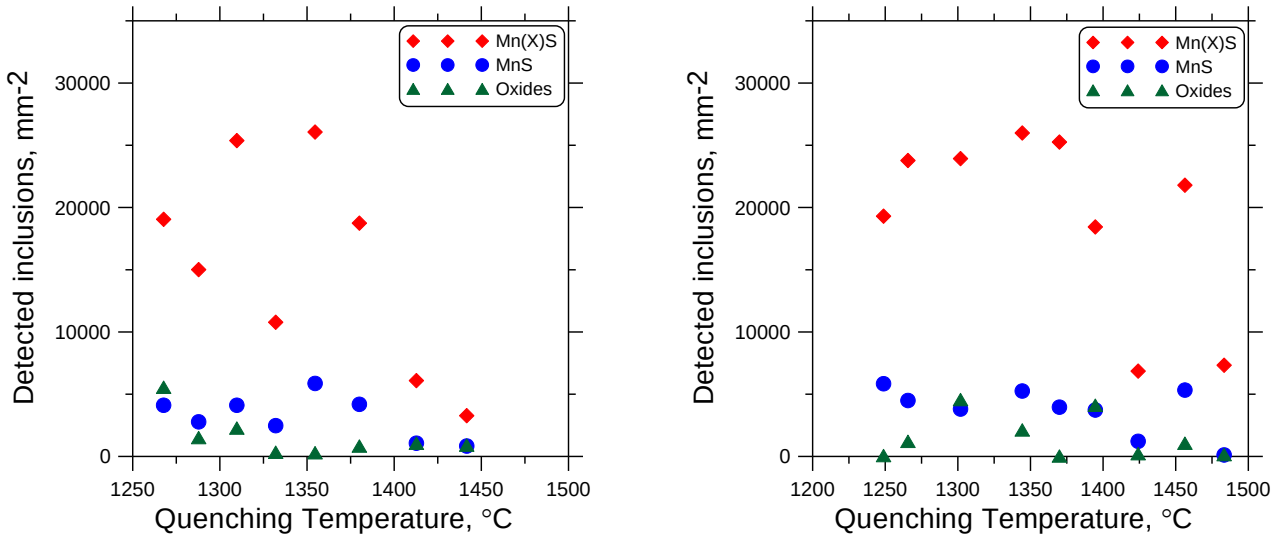

Fig. 2: Distribution of the MnS, Mn(X)S and oxides at different quenching temperatures. 3.4%C (left), 3.7%C (right).

The investigated samples have a fully martensitic microstructure. It is believed that the majority of the MnS and Mn(X)S inclusions were not existed in the melt at high superheat temperatures but these inclusions were formed in the chilled samples due to the non-equilibrium solidification conditions.

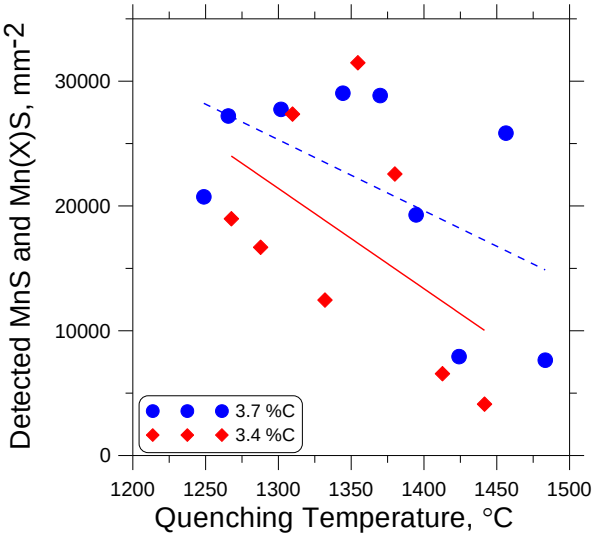

Fig. 3: The number of MnS and Mn(X)S inclusions at different quenching temperatures and carbon composition.

Lower quenching temperatures provide higher cooling rates. The number of the detected MnS and Mn(X)S inclusions is found to increase with increasing carbon content and decreasing cooling rates (lower quenching temperatures), see Figure 3. Due to the fact that MnS and Mn(X)S inclusions can serve as nucleation sites for the graphite can be concluded that as the number of these inclusions increases, earlier precipitation of graphite can occur, resulting to larger eutectic cells. This observation can explain partly the results of a previous work [14] where the eutectic cell size was found to increases with increasing carbon content.

It should be noticed that the graphite nucleation is a complex process which involves many different parameters and phenomena. For example the size of the eutectic cells depends on numerous parameters such as the secondary dendrite arm spacing (SDAS) [15] or the chemistry of the formed inclusions [7]. The present work aims to provide supplementary data to the existing knowledge.

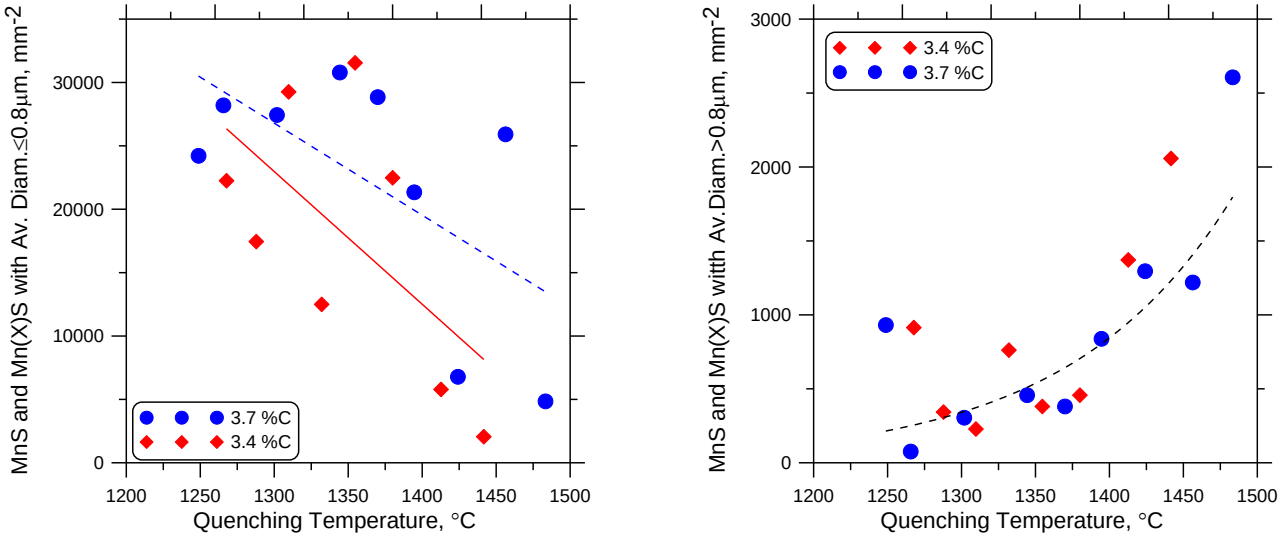

Fig. 4: Distribution of the MnS and Mn(X)S with size smaller or equal to 0.8µm (left) and with size larger of 0.8µm (right) at different quenching temperatures.

The average diameter of each inclusion was calculated as the diameter of a circle having area equal to the inclusion area. The increasing quenching temperature leads to a higher number of MnS and Mn(X)S inclusions with diameter smaller or equal to 0.8µm, see Figure 4 (left). On the other hand the higher number of MnS and Mn(X)S inclusions, having an average diameter larger than 0.8µm, were detected at high supercooling temperatures (lower cooling rates), Figure 4 (right). The later observation indicates the effect of cooling rate on the number of the of the large MnS and Mn(X)S inclusions. It has been proposed [16-17] that inclusions with radius larger than a critical radius can act as effective nucleation sites. Additionally in lamellar graphite iron the constitutional undercooling decreases with the reduction of the solidification rate [18]. Thus it appears that the absence of adequate number of large inclusions probably contributes to the increasing undercooling at high solidification rates in lamellar graphite iron.

Conclusions

1. Large number of MnS and Mn(X)S particles was found to exist at temperatures much higher than the predicted from the thermodynamic calculation. It is thought that these inclusions are the result of non-equilibrium cooling conditions.
2. Higher carbon content gives higher number of MnS and Mn(X)S particles and hence provides more potential nucleation sites for the precipitation of the graphite.
3. In view of the fact that higher quenching temperature provides lower cooling rates, the observed dependency between quenching temperatures, number and size of MnS and Mn(X)S, suggests that at lower cooling rates the number of the relatively large (>0.8µm) particles increases and thus the number of the particles that can act as effective nucleus for the graphite precipitation also increases.

References

1. I. Minkoff: ´The physical metallurgy of cast iron´, Jonh Wiley and sons, NY, 1983.
2. D.M. Stefanescu: *Materials Science and Engineering A*, 2005, 322-333.
3. R.B. Gundlach, J.F. Janowak, S. Bechet, K. Röhrigt: International symposium on the physical metallurgy of cast iron, ´The physical chemistry of inoculation of cast iron´, Stockholm 1984.
4. J. Tartera: *AFS International Cast Metals Journal*, 198, 7-14.
5. B. Lux, Recent research on Cast Iron, Edward Arnold Ltd, London, 1968, 241-288.
6. W. Weis: The Metallurgy of Cast Iron. St. Saphorin: Georgi Publishing Co, 1974, 69-79.
7. T. Skaland, O. Grong, T. Grong: Metallurgical Trans. A, 24A, 1993, 2321-2344.
8. J. F. Wallace, R. D. Rosemont: Conference on Modern Inoculating Practices for Gray and Ductile Iron, Illinois 1979, 41-73.
9. A. Sommerfeld, B. Tonn: *International Journal of Metalcasting*, vol 3, issue 4, 2009, 39-47.
10. I. Riposan, M. Chisamera, S. Stan, T. Skaland: AFS Cast Iron Inoculation Conference, Schaumburg Illinois, 2005, 31-41.
11. A. Velichko: Quantitative 3D characterization of graphite morphologies in cast iron using FIB microstructure tomography, Dissertation thesis work, University of Saarlandes, 2008, 103-110.
12. H.M. Mohmond, H. Fredriksson: *Metall. Trans. B*, 2012.

13. F. Schamber, Introduction to automated particle analysis by focused electron beam, Aspex Corporation, 2004.
14. V. Fourlakidis, L.V. Diaconu, A. Diószegi: Solidification and Gravity V, Trans Tech Publications, Switzerland, Materials Science Forum 649, 2010, 511-516.
15. A. Diószegi, K.Z. Liu, I.L. Svensson: *Int. J. Cast Met. Res*., 20.2, 2007, 68-72.
16. W. Kurz and D. Fisher: Fundamentals of solidification, 3rd edition, Trans Tech Publications, Switzerland, 1989.
17. A.L. Greer, A.M. Bunn, A. Tronche, P.V. Evans, D.J. Bristow: *Acta mater*., 2000, 48, 2823.
18. I. L. Svensson, A. Millberg; A. Diószegi, *Int. J. Cast Met. Res*., 2003, 16, 29-34.

Acknowledgements

The present work is a part of the research project JÄRNKOLL within the Casting Innovation Centre, financed by the Swedish Knowledge Foundation. Cooperating parties in the project are Jönköping University, Swerea SWECAST AB, Scania CV AB and Volvo Powertrain AB. Participating persons from these institutions/companies are acknowledged.